DTU Library

Effect of Graphene Oxide Thin Film on Growth and Electrochemical Performance of Hierarchical Zinc Sulfide Nanoweb for Supercapacitor Applications

Iqbal, Muhammad F.; Mahmood-Ul-Hassan; Razaq, Aamir; Ashiq, Muhammad N.; Kaneti, Yusuf; Azhar, Azhar A.; Yasmeen, Farhat; Joya, Khurrum Saleem; Abbass, Shafqat

Accepted Article

Authors: Muhammad Faisal Iqbal, mahmood ul Hassan, Aamir Razaq, Muhammad Naeem Ashiq, Farhat Yasmeen, Khurrum Saleem Joya, Shafqat Abbass, Yusuf Valentino Kaneti, and Azhar Alowasheeir Azhar

Excellent Effect of Graphene Oxide Thin Film on Growth and Electrochemical Performance of Hierarchical Zinc Sulfide Nanoweb for Supercapacitor Applications

Muhammad Faisal Iqbal*[abc], Dr. Mahmood-Ul-Hassan[a], Dr. Aamir Razaq[d], Dr. Muhammad Naeem Ashiq*[e], Dr. Yusuf Valentino Kaneti[b], Azhar Alowasheeir Azhar[b], Dr. Farhat Yasmeen[f], Dr. Khurrum Saleem Joya[f,g,h], Shafqat Abbass[e]

[a] Materials Growth and Simulation Laboratory, Department of Physics, University of The Punjab, Lahore 54590, Pakistan

[b] International Center for Materials Nanoarchitectonics (MANA), National Institute for Materials Science (NIMS), 1-1 Namiki, Tsukuba, Ibaraki 305-0044, Japan

[c] Department of Physics, Lahore Garrison University, Sector C, DHA Phase-VI Lahore, Pakistan

[d] Department of Physics, COMSATS Institute of Information Technology, Lahore 54000, Pakistan

[e] Institute of Chemical Sciences, Bahauddin Zakariya University, Multan 60800, Pakistan

[f] University of Engineering and Technology, Institute of Environmental Engineering and Research, GT Road, 54890 Lahore, Punjab, Pakistan

[g] Department of Energy Conversion and Storage, Denmark Technical University (DTU), Roskilde, Denmark

[h] Department of Chemistry, King Fahad University of Petroleum and Minerals (KFUPM), Dhahran, Saudi Arabia

* = Corresponding Author

E-mail: faisal.phd.physics@pu.edu.pk (Muhammad Faisal Iqbal), naeembzu@bzu.edu.pk, (Muhammad Naeem Ashiq), khurramdtu@gmail.com (Khurram S Joya)

Phone #: +92-300-9879344

Fax #: +92-61-9210068

1

Graphical Abstract

$$ZnS + KOH \longleftrightarrow ZnSOH + e^{-1} + K^{+1}$$
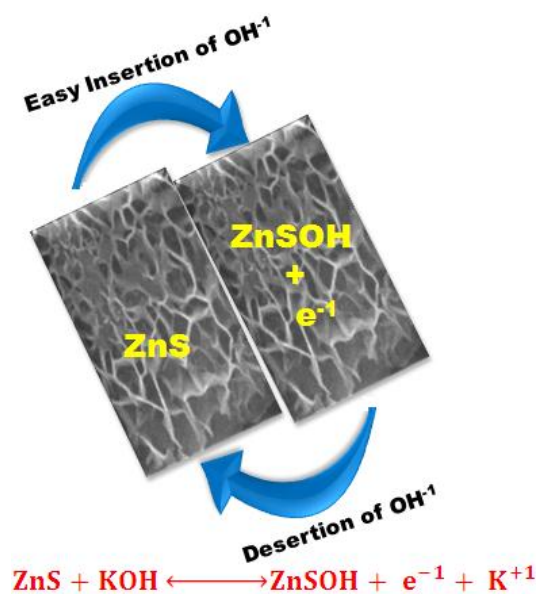
Abstract

Surface morphological induced electrical conductivity and specific surface area of a material play a significant role to facilitate electrochemical behavior for supercapacitors applications. Therefore, the synthesis step for controlling such parameters becomes very imperative and challenging. Herein, ZnS nanoweb is deposited directly on Ni foam having pre-deposited graphene oxide thin layer developed via hydrothermal method. The structure and surface morphology of modified ZnS is observed using, respectively, XRD and SEM. The electrical conductivity determined for graphene oxide supported ZnS nanoweb, using four probes method, is 100.15 Scm^{-1}, while the specific surface area is 104.42 m^2g^{-1} by BET measurements. Pseudocapacitive behavior is monitored by cyclic voltammetry, and the excellent specific capacity of 3052 Fg^{-1} has been found at the scan rate 2 mVs^{-1}, while it is 2400.30 Fg^{-1} according the galvanostatic charge-discharge profile at (current density) 3 $mAcm^{-2}$, which significantly higher than those measured for bare GO or ZnS layers. The energy and power densities of GO supported ZnS nanoweb, determined using three electrode systems, are 120 $WhKg^{-1}$ at 3 $mAcm^{-2}$ and 4407.73 Wkg^{-1}, respectively. The symmetric

2

behavior using two electrode systems show an energy density 20.29 WhKg^{-1} at 2 mAcm^{-2}. Hence, both symmetric and asymmetric measurements suggest that GO supported ZnS nanoweb can be applied as the suitable electrode for supercapacitors.

Keywords: Energy Density; Graphene oxide; Specific Capacitance; Supercapacitor; Zinc Sulfide

1. Introduction

Energy storage devices have been proven backbone for addressing the existing energy crises and for supplying energy during shutdown of the traditional electricity. Energy storage devices are most suited to supply energy to various electronic devices, electrical vehicles and heavy industries.[1-4] Among the various existing devices involving various energy storing mechanisms e.g., batteries, traditional capacitors, supercapacitors and the fuel cell etc., the supercapacitors are considered most attractive due to their light weight, low price and high capacitance, capability for simultaneously maintaining the both energy and power density and significantly large life cycles. [2, 5-7] The main categories of supercapacitors, which is dependent upon the existing energy storage phenomena, are electric double layer supercapacitors (EDLCs) and pseudocapacitors. In the first category, an electrochemical double layer formed by electrolyte ions appears at the electrode surface instead of the electronic flow between the electrolyte and electrode surface. In contrast, this second category involves faradaic reaction at the electrode surface. [8-10]

The electrochemical nature of the investigated electrode is fundamental because it decides the efficiency of a supercapacitor. Different materials including carbonaceous, polymers, metal oxides, metal organic framework (MOFs), metal sulfides and different composites, have been investigated to expose the potential electrode applications in supercapacitors. [11-15] However, due to various limitations in the materials, practical

3

applications are restricted. For example, carbonaceous electrodes are suited only for EDLCs with low specific capacitance, oxides and MOFs (expensive and difficult fabrication) exhibit poor electrical conductivity. [8, 16-20] Although metal sulfides show fairly well electrical conductivity but the electrochemical performance can be further enhanced by realizing higher electrical conductivity and specific surface area values. Carbonaceous materials (e.g., graphene oxide (GO)), exhibit a variety of potential applications, e.g., photoelectrocatalytic activity and vivo-bio imaging, which are due to the large specific surface area and high electrical conductivity. [21-24] Hence, with the use of GO, the improved electrochemical nature of the electrodes in supercapacitors could be anticipated. [2, 3, 25, 26] Furthermore, the extensive literature survey shows scarcity of the reports on metallic sulfides for electrochemical applications but they faced problems with electrode stability which can be improved by transition metal sulfides. [27, 28]

Herein, GO thin layer was initially prepared on a flexible nickel foam (NF), and then ZnS nanoweb were deposited on it using hydrothermal route. The structure and surface characteristics were explored using X-ray diffraction (XRD) and scanning electron microscopy (SEM), respectively. Elemental atomic ratio was observed by energy dispersive X-ray technique (EDX). Moreover, the electrical conductivity exhibited, the stabilized specific surface area and the measured electrochemical natures of individual ZnS on NF have been contrasted with those for GO supported ZnS nanoweb on NF substrate to elucidate the practical significance of the designed system.

2. Results and Discussion

The XRD pattern of GO supported ZnS synthesized on NF substrate measured using X-ray diffractometer (Rigaku Smart lab) is depicted in Fig. 1. The diffraction peaks appeared at 10.40°, 28.90°, 44.41°, 51.93° and 76.38°. The diffraction peak at 10.40° are indicative of GO, while 2θ values at 28.90°, 51.93° and 76.38° were assigned to the hexagonal ZnS

4

crystallographic planes (0 0 2), (1 0 3) and (2 1 0), respectively, which was decided due to

consistency with JCPDS card no. 00-001-0677. Moreover, the diffraction peaks appearing at

44.41° and the shoulder of the diffraction peak at 76.38° are originating from NF substrate.

Similarly, individual ZnS fabricated on NF substrate exhibited a similar XRD pattern (see

Fig. S1 in the supporting file), however the GO peak was absent expectedly, confirming the

accuracy of the XRD pattern (Fig. 1).
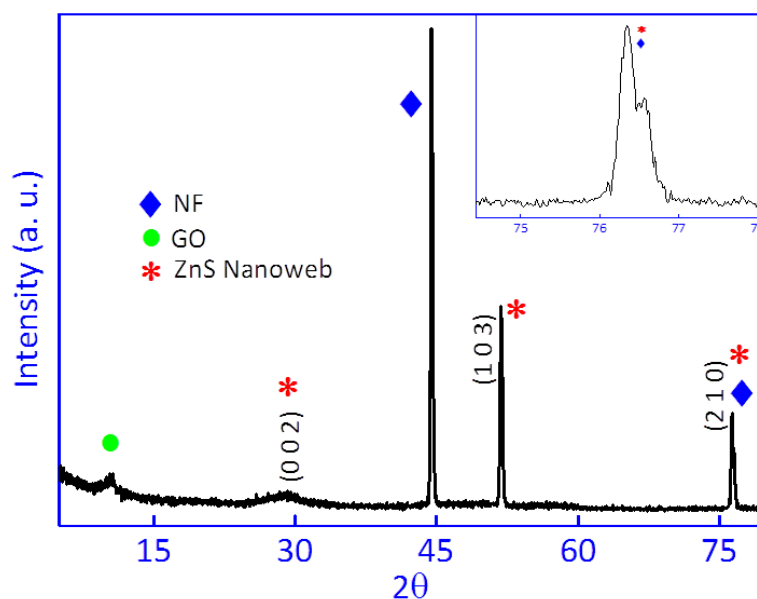
Figure 1: XRD pattern of GO supported ZnS nanoweb prepared on a NF substrate.

Surface morphology is a significant feature because it critically affects the specific properties

of material for certain applications. The surface morphological study of GO supported ZnS

nanoweb and individual ZnS fabricated on nickel foam (NF) substrate was conducted using

scanning electron microscopy (SEM) and the measured images are shown in Fig. 2. The

surface morphology of NF and GO thin observed by using SEM has been given in Fig. S2.

GO thin film showed some cracks arising due to the porous nature of NF. The measured SEM

images, shown in Fig. 2 (a & b) with two different magnifications, illustrated nanoweb like

surface morphology of the GO supported ZnS fabricated on NF substrate. On the other hand,

surface morphology of the ZnS directly fabricated on bare NF, as shown in Fig. 2 (c &d)

5

exhibited nano granular structure having broad variations in the size and shape. Hence, it was evident that GO thin film adsorbed on to the NF substrate created large active sites for the good adhesion of ZnS and resulting in the nanoweb like surface structure. [29]

Elemental mapping of GO supported ZnS and individual ZnS has been carried out by Fe-SEM with EDX (SU8000). EDX elemental mapping correspond that atomic ratio of Ni, C, Zn and S in GO supported ZnS nanoweb electrode was 47.39, 43.17, 6.41 and 3.03 % (Fig. 2 (e)). While in case of individual ZnS, atomic ratio of Ni, Zn and S was 76.91, 14.10 and 9.00 % (Fig. 2 (f)). As atomic ratio of Zn and S was higher in individual ZnS, which may be due to porous type nature of nickel foam substrate but it was covered by GO in composite form as GO supported ZnS nanoweb.
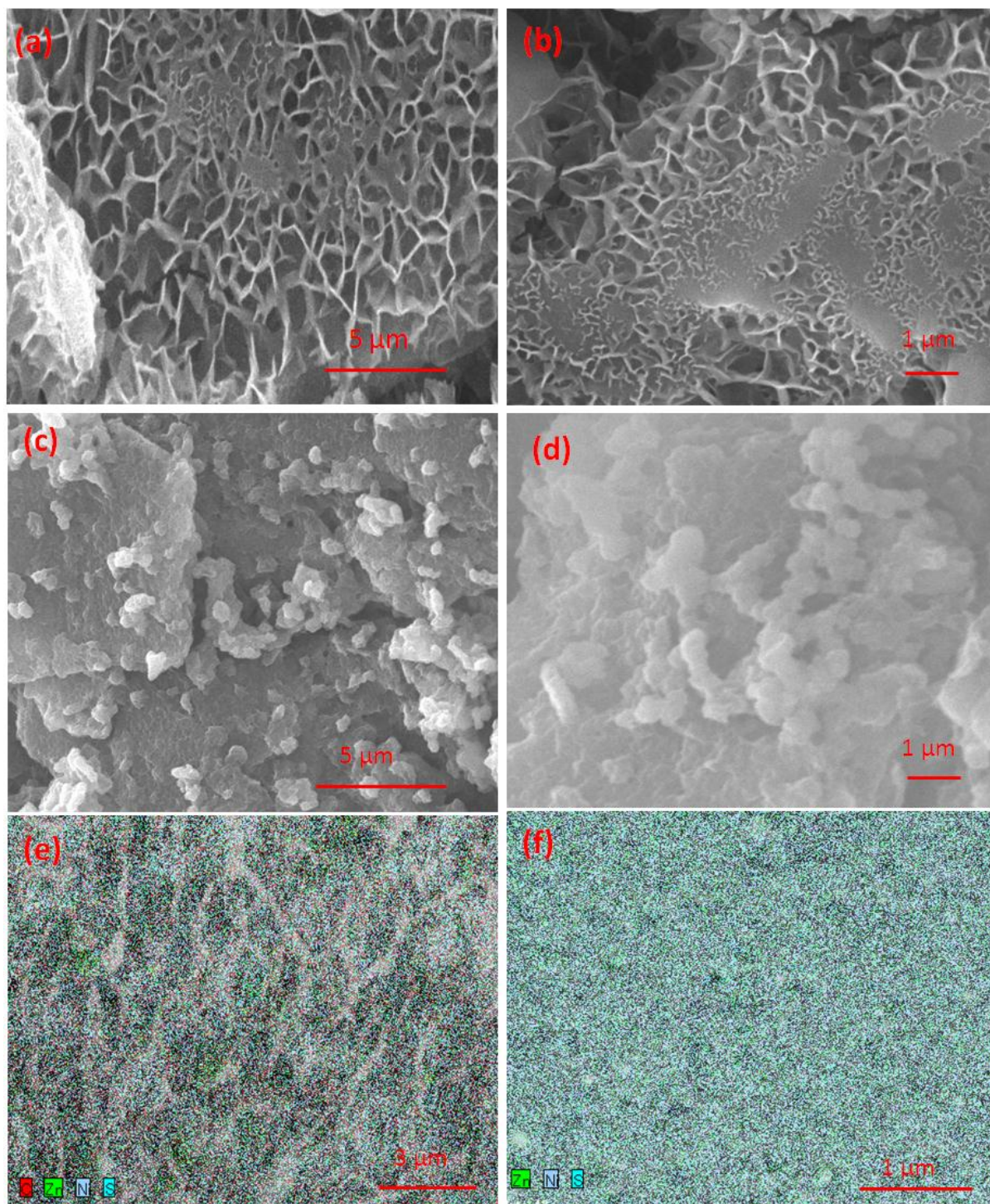
Accepted Manuscript

6

Figure 2: SEM images measured at two different magnifications for (a & b) GO supported ZnS nanoweb on NF substrate and (c & d) individual ZnS grains. EDX mapping for (e) GO supported ZnS nanoweb and (f) individual ZnS on NF substrate.

7

The electrical conductivity of individual ZnS and GO supported ZnS nanoweb is measured using four-probe technique to know the electrochemical nature of the electrodes for supercapacitors application. The electrical conductivity measured for individual ZnS and GO supported ZnS nanoweb on NF was 43.46 and 100.15 Scm^{-1}, respectively. As apparent from the measured conductivity values, the GO being a good conducting material enhances the conductivity of ZnS nanoweb developed on it, relative to ZnS, which showed less electrical conductivity while being a semiconductor. [30] It is assumed that the presence of GO under layer resulted an easy charge carrier flow through the ZnS nanoweb structure that enhanced the electrical conductivity. As GO is characterized as having p-type nature, while ZnS exhibits n-type semiconducting character, therefore, at their interface Fermi level needs shifting causing carrier flow, owing to which the electrical conductivity of ZnS nanoweb is enhanced. [27]

The specific surface area of GO supported ZnS nanoweb and simple ZnS prepared on NF substrate has been determined by N$_2$ absorption/desorption isotherms curves (See Figure S3) at 77K using BET method. The specific surface area was 104.42 m^{2}g^{-1} for GO supported ZnS nanoweb and 75.83 m^{2}g^{-1} for individual ZnS. GO grows two dimensionally (2D) with large specific surface area, therefore, it increased the specific surface area of ZnS nanoweb deposited on it, which is suitable for high electrochemical performance. [31, 32]

2.1 Electrochemical Testing by Three electrodes

The electrochemical testing are performed using three electrodes system to elucidate the electrochemical behavior of individual ZnS layer and GO supported ZnS nanoweb. Hence, potential supercapacitor applications can be evaluated. The electrochemical performance of the fabricated GO thin film has been already reported in a previous report. [27] GO has found playing effective character for optimizing the electrochemical nature of the metal sulfide layer. [27] The cyclic voltammetry (CV) was performed in a 2M KOH electrolyte, and the CV

8

curves measured at different scan rates are plotted in Fig. 3. It is quite evident from Fig. 3 (a) that individual ZnS showed good redox peaks in potential window 0.0-0.60 V revealing its pseudocapacitive behavior. [33] The specific capacitance, as determined using CV plots, was calculated using Eq. 1,

$$C_s = \frac{\int_{V_c}^{V_a} I * dV}{m * S * \Delta V} \qquad (1)$$

Where, I and dV express current and the potential values extracted from the redox peaks. The symbols m, S and ΔV express the fabricated active mass, the scan rate applied and the potential window set for the CV test. The measured specific capacitance of individual ZnS was 1240.62, 1200.43 and 1040.80 Fg^{-1} at 2, 5 and 10 mVs^{-1}, respectively. Fig. 3 (b) shows the CV graphs measured for GO supported ZnS nanoweb fabricated on NF substrate. The CV curve measured for ZnS nanoweb exhibited well resolved redox peaks, however, potential was slightly shifted to a higher regime with the increasing scan rate (2, 5, 10, 15 and 20 mVs^{-1}), suggesting pseudocapacitive behavior of the material. [34] Thus, GO supported ZnS nanoweb exhibited significantly large CV behavior and greater potential window as compared to those shown by individual ZnS. Moreover, a potential window of 0.8 V was found for GO supported ZnS nanoweb, which is greater than many reported works. [30] Such a larger potential window of GO supported ZnS nanoweb is attributed to more thermodynamically active available GO sites relative to individual ZnS. Fig. 3 (c) shows the redox current at various scan rates that increased linear against square-root of scan rate, confirming the pseudocapacitor like nature for GO supported ZnS nanoweb. [35] The GO supported ZnS nanoweb also showed excellent specific capacitance of 3052, 2625.82 and 2105.70 Fg^{-1}, respectively, at 2, 5 and 10 mVs^{-1}, larger than that by the individual ZnS electrode. Such a large improvement might be originated due to the nanoweb like surface structure, associated with the higher electrical conductivity values as well as the greater specific surface area. [36]
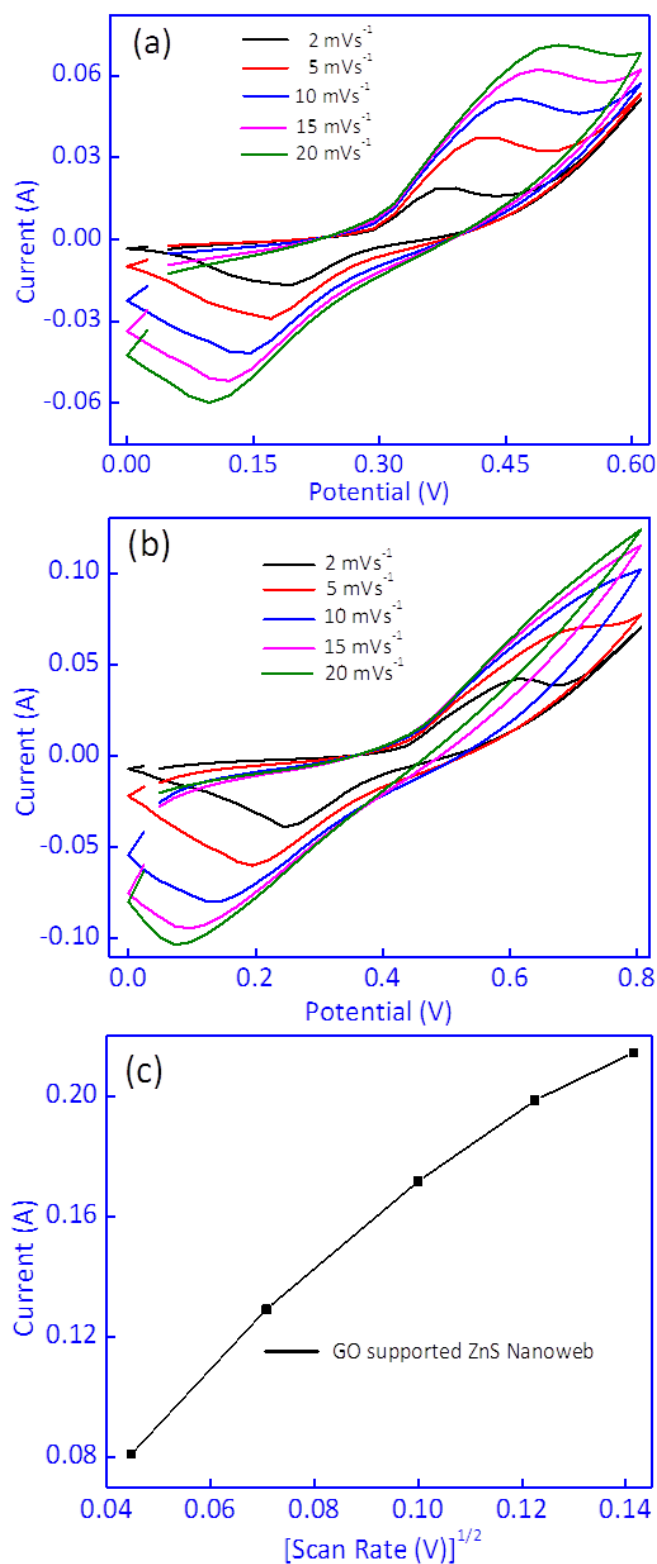
9

Figure 3: The CV curves measured for (a) individual ZnS and (b) GO supported ZnS nanoweb. (c) The linearly increased redox current as function of square root of the scan rates for GO supported ZnS nanoweb.

The galvanostatic charge-discharge (GCD) profile for individual ZnS and GO supported ZnS nanoweb using three electrode systems is shown in Fig. 4. As evident from Fig. 4 (a), the GCD profile for only ZnS showed discharge time 471s, 230s, 150s and 94s at (current densities) 3, 5, 10 and 15 mAcm^{-2}, respectively. The specific capacitance C_s of individual ZnS on NF substrate was calculated using the following Eq. 2,

$$C_s = \frac{I}{m * \frac{dV}{dt}} \qquad (2)$$

Where, dV/dt expresses the slope region in the GCD curve, m represents the active mass per cm of the electrode material and I is the current applied during GCD test. The calculated specific capacitance for individual ZnS was 1296.51, 1334, 1055.18 and 922.50 Fg^{-1}, respectively, at 3, 5, 10 and 15 mAcm^{-2}. The energy (E_d) and power densities (P_d) were calculated using Eq. 3 & 4, respectively. [37]

$$E_d = 0.5 \, C_s (\Delta V)^2 \qquad (3)$$

$$P_d = \frac{E_d}{t} \qquad (4)$$

Where, ΔV and t represents potential window and discharge time, respectively. The energy density for individual ZnS was 45, 46.32, 37 and 32 WhKg^{-1} at the current densities 3, 5, 10 and 15 mAcm^{-2}, respectively. The individual ZnS showed maximum C_s of 1334 Fg^{-1} and an energy density 46.32 WhKg^{-1} was measured at the current density 5 mAcm^{-2}. The individual ZnS exhibited power density of 344, 725, 887.65 and 1226.70 WKg^{-1} at energy density 45, 46.32, 37 and 32 WhKg^{-1}, respectively.

The GO supported ZnS nanoweb showed excellent electrochemical properties indicating its suitability as electrode material for supercapacitors applications. Fig. 4 (b) revealed GO supported ZnS nanoweb exhibit good discharge times of 592, 321, 181 and 95 s, at 3, 5, 10 and 15 mAcm^{-2}, respectively. A large plateau region in CV curves confirmed the pseudocapacitive behavior of GO supported ZnS nanoweb fabricated on the NF substrate. [34,

11

[38, 39] The specific capacitances and energy densities were measured using Eq. 2 & 3, respectively. The specific capacitance and the energy densities measured for GO supported ZnS nanoweb electrode at the current densities 3, 5, 10, 15 mAcm^{-2} were found as 2400.30, 2345.70, 2219, 2326.31 Fg^{-1} and 120, 117.30, 111, 116.32 WhKg^{-1}, respectively. Both the specific capacitance as well as the energy density measured for GO supported ZnS nanoweb were found significantly larger than that by the GO layer and individual ZnS prepared on NF. The enhanced values might be appeared due to the mechanical support offered by the GO thin film causing the ZnS nanoweb to exhibit delayed discharging character, and hence, improved electrochemical behavior was resulted. [16, 17, 34] Moreover, the large electrical conductivity of ZnS nanoweb facilitated the easy electronic transfers at the electrode surface, which showed optimized electrochemical behavior. The charge transfer resulting in charge storage mechanism is shown in below scheme. [30, 40]

$$ZnS + KOH \longleftrightarrow ZnSOH + e^{-1} + K^{+1}$$
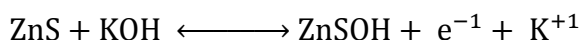
The GO supported ZnS nanoweb showed maximum specific capacitance and energy density 2400.27 Fg^{-1} and 120 WhKg^{-1}, respectively, at 3 mAcm^{-2}. However specific capacitance and energy density were decreased with the current density, which illustrated that higher excitation result GO supported ZnS nanoweb to exhibit large polarization and become more resistive for the electrolyte ion diffusion or the charge transfer. [16, 40, 41] Furthermore, the measured higher electrochemical parameters were also found related to the improved electrical conductivity and specific surface area of GO supported ZnS nanoweb as compared to the ZnS fabricated on NF. [42] The measured specific capacitance was excellent and much larger than previously reported materials (see Table 1). Similarly, energy density of GO supported ZnS nanoweb was also found much higher than those in many previous reports. [34,

[38, 43-45] The GO supported ZnS nanoweb electrode delivered power density 730, 1315.34, 2206.63 and 4407.73 WKg^{-1} at the energy density 120, 117.30, 111 and 116.32 $WhKg^{-1}$, respectively. The maximum power density 4407.73 WKg^{-1} was found very high as compared to those in the reported literature. [34, 40, 45] The results suggested that ZnS nanoweb prepared on GO layer acting as the electrode exhibit excellent electrochemical behavior suitable for applications in asymmetric supercapacitor.

Table 1: Comparison of specific capacitance GO supported ZnS nanoweb electrode measured at various electrochemical parameters of using three electrode GCD systems other electrode materials.

S. no	Material	Substrate	Solution M KOH	Current density	C_s (Fg^{-1})	Reference
1	ZnS/G Nanocomposites	NF	6	5 mVs^{-1}	197.1	30
2	CoS	NF	6	1 Ag^{-1}	564	46
3	Ni−Co−S-6	NF	6	2 Ag^{-1}	1304	47
4	CC-NC-LDH Hybrid	Carbon Cloth	6	1 Ag^{-1}	1817	48
5	TP-NixSy/rGO	NF	2	1 Ag^{-1}	2074	49
6	$NiCo_2S_4$/MWCNTs	NF	6	1 A/g	2080	43
7	NiS	NF	6	1 Ag^{-1}	2112	50
8	GO supported Al_2S_3 nanorambutan	NF	2	3 $mAcm^{-2}$	2178.16	40
9	GO supported ZnS nanoweb	NF	2	3 $mAcm^{-2}$	2400.30	This work
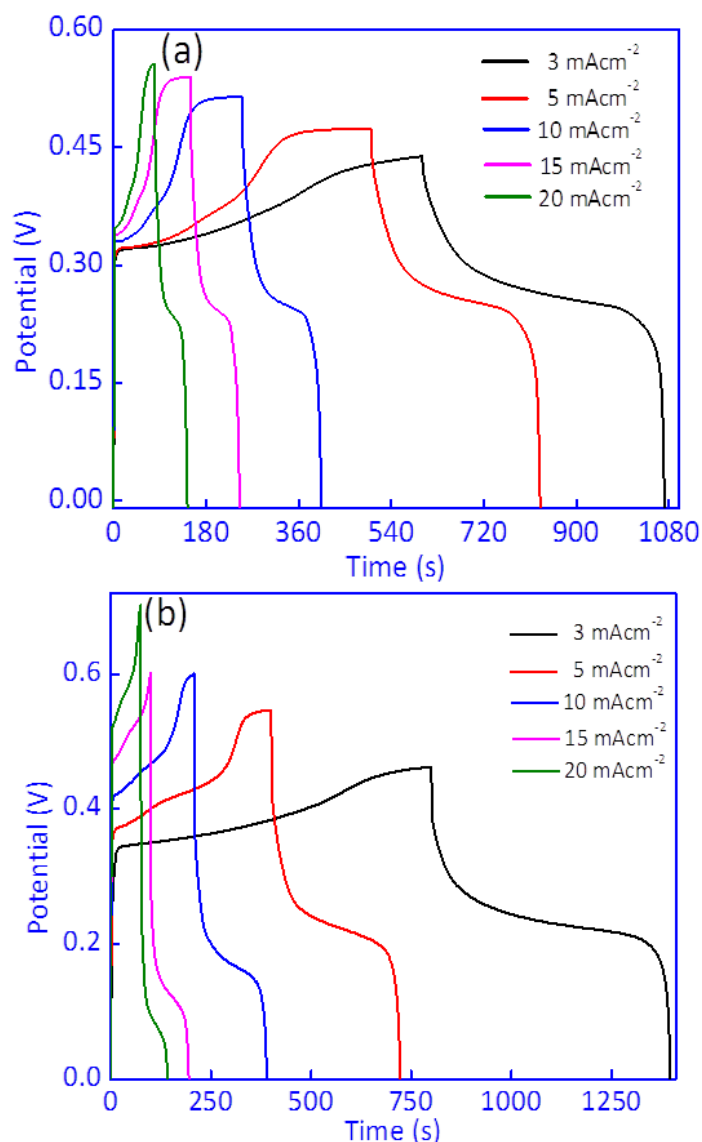
Figure 4: Galvanostatic charge-discharge profile of (a) individual ZnS and (b) GO supported ZnS nanoweb on NF under varying current density.

Nyquist plot presented in the Fig. 5 (a) illustrates the real resistance Z' versus imaginary parts Z'' of electrochemical impedance for GO supported ZnS nanoweb and individual ZnS. Observed equivalent series resistance was 1.56 and 2.96 Ω for GO supported ZnS nanoweb and individual ZnS individual ZnS on NF substrate, which corresponds series equivalent resistant for individual ZnS was greater than GO supported ZnS nanoweb. The zoom area of inset Fig. 5 (a) reveals to smaller kink at the high frequency region for GO supported ZnS

14

nanoweb corresponds to a small semicircle, which indicates very smaller contact and charge resistances. The straight line in the low frequency region exhibits a slope higher for GO supported ZnS nanoweb as compared to the individual ZnS (Fig. 5 (a)) at the same conditions. Such a larger slope represents smaller Warburg resistance. Hence, the use of GO thin film improved the conductive network of ZnS nanoweb and making it more suitable for electrochemical applications. Such GO mediated enhancement in the electrical conduction was also found before consistent with the observation from CV and GCD curves in this study. The more conductive nature of ZnS nanoweb may be ascribed to the high electrical conductivity and greater effective surface area. 51

The electrode stability, of GO supported ZnS nanoweb and individual ZnS, was evaluated using CV curves (see Fig. 5 (b)). The electrode stability testing is mostly employed to observe the supercapacitor applcations. For example, Pujari et al. (2016) investigated the electrode stability of MnS nanofiber using CV analysis. Simmilarly Patil et al. (2017) employed the CV data for testing the electrode stability to evaluate the aymmetric supercapcitor applications of Co_3S_4/Co_3S_4-rGO. The GO supported ZnS nanoweb, even after 1000 cycles retained 95.90 % of the specific capacitance, while individual ZnS showed only 53.6 % retention. The excellent specific capacitance retention exhibited by GO supported ZnS nanoweb was attributed to the nanoweb like surface structure and significantly higher specific area, which can activate the electrode for conduction, in contrast to that in the individual ZnS. 44, 52 Structural stability was also observed by XRD after electrochemical testing as given in Fig. S4, which showed that although intensity has been reduced but peaks are still appeared at the same positions corresponding to GO supported ZnS nanoweb.
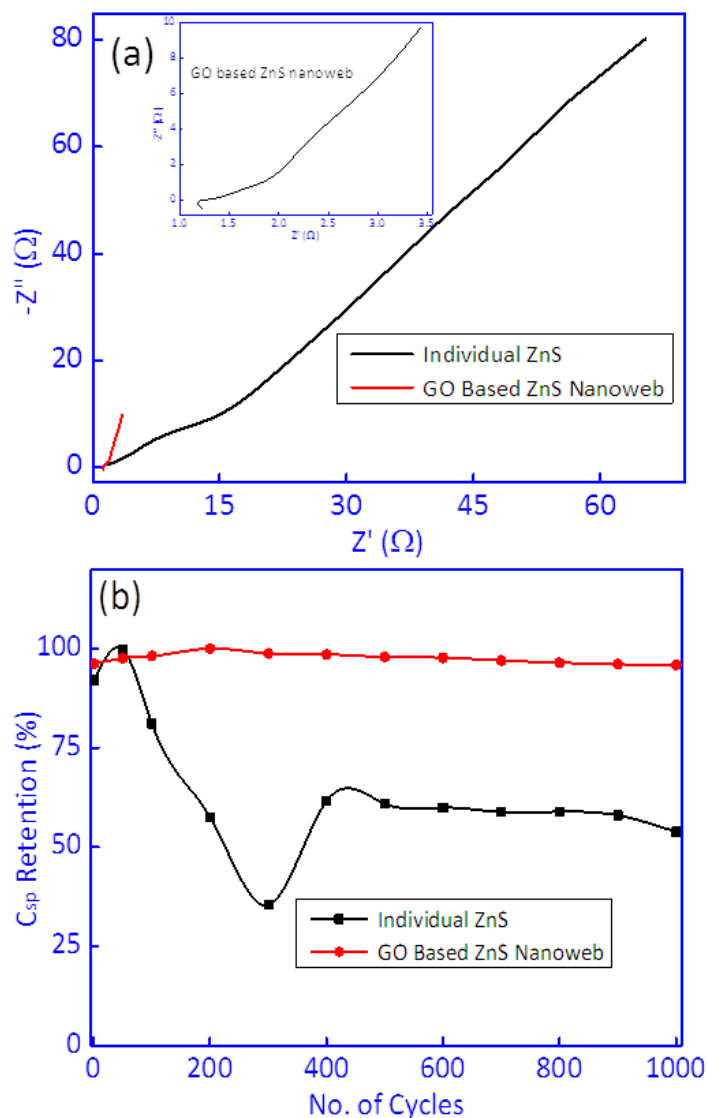
Figure 5: (a) Nyquist plot for GO supported ZnS Nanoweb and individual ZnS (b) electrode stability test for GO supported ZnS nanoweb and individual ZnS fabricated on NF substrate.

2.2 Two Electrodes Symmetric System

The electrochemical behavior was also elucidated using two electrode system for observing the symmetric supercapacitor applications. Two electrodes were formed using GO supported ZnS nanoweb, which were separated by the filter paper, sandwiched by the current collector (gold deposited Cu foil) and sealed into the coffee bag. The CV and GCD measurements using two symmetric GO supported ZnS nanoweb electrodes were performed with Autolab PGSTAT 12. Fig. 6 (a & b) shows CV curves at the scan rate 2, 5, 15 and 20 mVs^{-1} and GCD

16

curves at the current density 0.50, 1 and 2 mAcm^{-2}, respectively, for GO supported ZnS nanoweb on NF substrate. The measured CV curves (Fig. 6 a) revealed that GO supported ZnS nanoweb shows double redox peaks within -0.4 to 0.4 V confirming the pseudocapacitive character of this material. The double oxidation and reduction peaks showed that redox reactions occur two times, which was justified due to gold-plated Cu sheets employed for as the current sensor. Similarly, GCD profile (Fig. 6 b) also manifested two redox reactions for demonstrating the underlying pseudocapacitive behavior of GO supported ZnS nanoweb fabricated on NF substrate. The possible charge storage mechanism, as shown in Fig. 7, indicated that OH^{-1} moves easily from one electrode surface to another electrode, which may result because of the optimum conductivity and suitable large specific surface area of the electrode surface available during the charge and discharge process. [27] The specific capacitance was computed using the following Eq. 5. [49, 53]

$$C_s = \frac{2 * I}{m * \frac{dV}{dt}} \qquad (5)$$

The symbols m and I show the active mass of the electrode and the current applied during GCD. The specific capacitance determined for GO supported ZnS nanoweb was 131.30, 228.30 and 175.92 Fg^{-1} at the current density 0.50, 1 and 2 mAcm^{-2}, respectively. The GO supported ZnS nanoweb exhibited the maximum specific capacitance 228.30 Fg^{-1} at 1 mAcm^{-2}. It was found that GO supported ZnS nanoweb remains less active at the smaller current density, while it polarizes due to larger resistivity at higher current density. However, 1 mAcm^{-2} was appropriate for the efficiently excitation of the GO supported ZnS nanoweb associated with the suppressed polarization. The energy density determined for GO supported ZnS nanoweb, using Eq. 3, was 11.67, 20.29 and 15.64 WhKg^{-1} at current density 0.50, 1 and 2 mAcm^{-2}, respectively. The GO supported ZnS nanoweb exhibited the maximum energy density 20.29 WhKg^{-1} at 2 mAcm^{-2} using two electrode system. The larger energy density for

17

the GO supported ZnS, grown by a very simple and inexpensive growth method, illustrates an advantage over the molybdenum sulfide and nitrogen-doped carbon nanofibers supported flexible supercapacitor prepared using complicated synthesis technique, exhibited energy density 5.42 WhKg^{-1} and 10.96 WhKg^{-1}, as reported by Javed et al. (2015) and Chen et al. (2017), respectively. [2, 54] The GO supported ZnS nanoweb exhibited power density 154.50, 227.58 and 485.30 WKg^{-1} at the energy density 11.67, 20.29 and 15.64 WhKg^{-1}, respectively. The symmetric behavior of individual ZnS on NF substrate was also investigated under similar conditions, which is shown in Fig. 6 (c & d). Fig. 6 (c) shows CV curves measured for individual ZnS in the potential window -0.3 to 0.4 V at the scan rate 2, 5, 15 and 20 mVs^{-1}. It was found that individual ZnS also exhibit faradaic reactions similar to those observed for GO supported ZnS nanoweb. Interestingly, the potential window for GO supported ZnS nanoweb is higher than for the individual ZnS, and this observation similar that from the three electrode systems. Such improvement was found due to GO thin film that optimizes the surface morphological impacts and the electrical conductivity of ZnS nanoweb. Hence, the potential window for GO supported ZnS nanoweb was found equal to 0.8 V in both two and three electrodes system, however, a shift towards the positive region was also observed, suggesting that GO supported ZnS nanoweb is suitable for the supercapacitors operating for the positive potential window. The individual ZnS exhibited poor specific capacitance, energy density and power density as compare to GO supported ZnS nanoweb. The specific capacitance and the energy density determined for individual ZnS from the GCD profile (Fig. 6 d) was found as 102.45, 101.20, 72.64 Fg^{-1} and 6.97, 6.90, 4.94 WhKg^{-1} at 0.50, 1, 2 mAcm^{-2}, respectively. While the power density of individual ZnS was found as 102.88, 229.57 and 494.36 WhKg^{-1} at the energy density 6.97, 6.90 and 4.94 WhKg^{-1}, respectively.
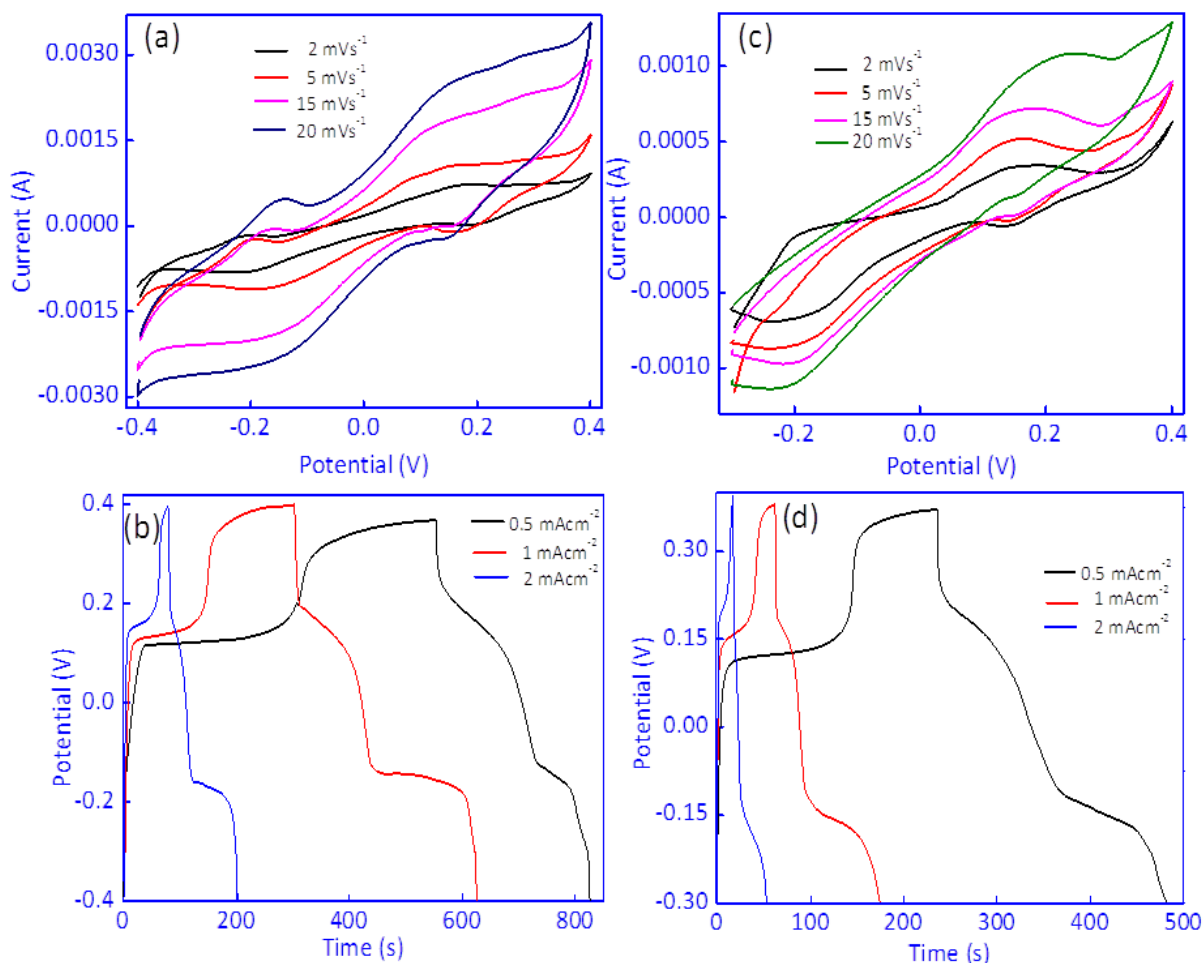
18

Figure 6: The (a) CV plots and (b) GCD profiles measured for GO supported ZnS nanoweb. The (c) CV plots and (d) GCD nature measured for individual ZnS on NF substrate. The measurements were performed using two electrodes symmetric system.

Owing to good two electrodes symmetric behavior of GO supported ZnS nanoweb endorsed to observe two electrodes stability and EIS test. Hence, two electrodes symmetric test for GO supported ZnS nanoweb was measured at same electrochemical conditions up to 1000 cycles (Fig. 6 (b)). Inset images showed the 1st, 500th and 1000th cycles, those revealed that the cyclic behavior changed with e passage of time. Stability curves revealed that C_s reduced abruptly up to 57 % in first 50 cycles, which might be due to some kind of activation of materials but later reduced slowly. C_s retention up to 450 cycles revealed 36 % but it retained up to 27 % after 100 cycles. After 50 cycles, the decreasing way of C_s suggested nearly linear

19

and good stability. EIS data (Fig. 7 (c)) revealed a huge semicircle in low frequency and straight line in high frequency region. Large semicircle showed series equivalent resistance of 497 Ω, so in symmetric behavior, the whole conduction was due to electrode structures instead of standard electrodes. Further the inset images showed the series equivalent circuit for GO supported ZnS nanoweb, it revealed the same solution resistance (R_s) and charge transfer resistance (R_{ct}) of 9.31 Ω. Capacitance and double layer capacitance was 3.77 and 634 uF respectively, while Warburg resistance was very small as 23.9 uΩ as straight line showed that Warburg resistance is small as compare to charge transfer and solution resistance.
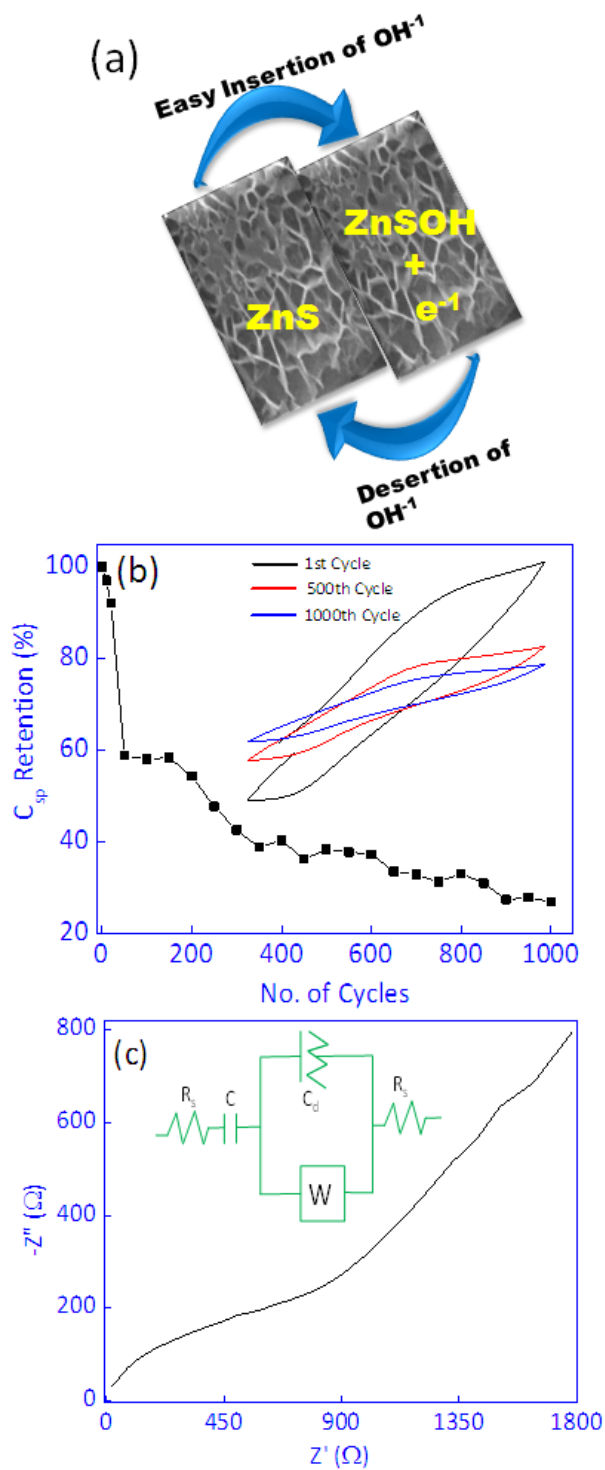
20

Figure 7: A schematic illustration of the charge storage mechanism in GO supported ZnS nanoweb (b) Electrode stability test and (c) electrochemical impedance spectroscopy for Symmetric GO supported ZnS nanoweb.

3. Conclusion

In supercapacitors applications, morphology of a material is a key parameter to enhance the electrical conductivity and specific surface area. We undertake here controlled synthesis of ZnS nanoweb deposited directly on thin layer graphene oxide (GO) modified Ni foam. The growth of ZnS (having nanoweb like surface observed using SEM) on the NF pre-deposited with GO layer was confirmed from the XRD analysis. The GO supported ZnS nanoweb was showed exhibiting good electrical conductivity 100.15 Scm^{-1} and the specific surface area 104.42 m^2g^{-1}. The excellent specific capacity 2400.30 Fg^{-1} and energy density 120 $WhKg^{-1}$ were measured at current density 3 $mAcm^{-2}$ using three electrode systems, while the power density 4407.73 WKg^{-1} was found at 15 $mAcm^{-2}$. The excellent electrochemical performance observed was justified due to the excellent value of the electrical conductivity, greater area of the effective surface. The two electrode symmetric measurements of GO supported ZnS nanoweb also gave good energy density 20.29 $WhKg^{-1}$ at 2 $mAcm^{-2}$. Hence, both symmetric and asymmetric measurements of GO supported ZnS nanoweb suggested it as the most excellent electrode for supercapacitor applications.

4. Experimental Section

Modified Hummers and Offenmans method was applied for fabrication of GO and thin film on nickel foam substrate was deposited through using ultra-sonication, for details see our previous work. [27] The GO supported ZnS nanoweb was finally synthesized using hydrothermal process. For the hydrothermal synthesis, 0.05 M $Zn(CH_3COO)_2.H_2O$ solution was prepared in a canonical flask and 0.05M K_2S solution was added drop-wise using burette under continuous stirring at magnetic stirrer. The NF having GO thin layer was also immersed into the solution. The formed precipitates and the immersed NF having pre-deposited GO were transferred to a Teflon lined stainless steel autoclave that was subjected to 150 ℃ for 4 h using an electric oven. A schematic illustration showing this synthesis process

22

is given as Fig. 8. The final fabricated product on NF with pre-deposited GO after washing with deionized water was dried at 50 ºC in electric oven. Moreover, individual ZnS was also prepared on bare (without GO thin film) NF substrate under similar conditions. Active mass were measured as 2.7, 4.8 and 6.2 mg per cm^2 for GO thin film, individual ZnS and GO supported ZnS, respectively. A reaction resulted the formation of ZnS could be expressed as:
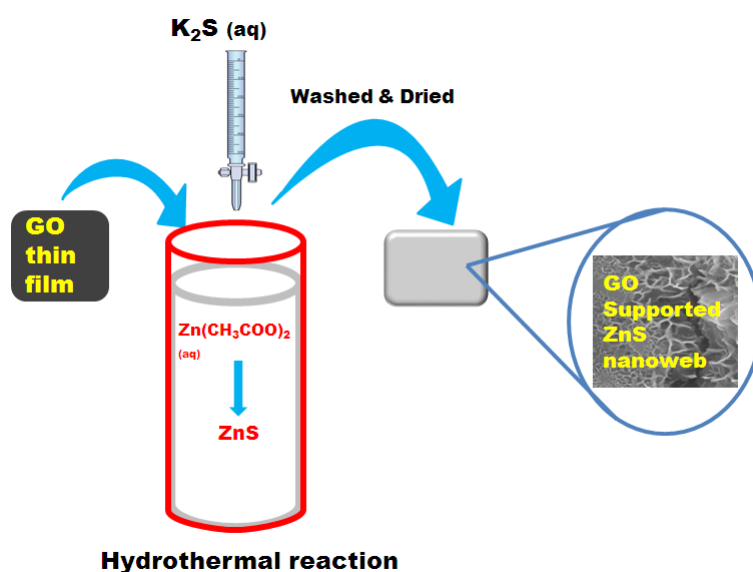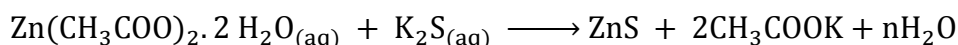
$$Zn(CH_3COO)_2 . 2\,H_2O_{(aq)} \ + \ K_2S_{(aq)} \ \longrightarrow \ ZnS \ + \ 2CH_3COOK + nH_2O$$

Figure 8: Synthesis process for GO supported ZnS nanoweb

4.1 Characterization

The structural properties were revealed using X-ray diffractometer (Rigaku Smart lab) by employing CuK$_\alpha$ X-rays within 2θ range 5-80˚. The surface study was carried out using SEM (JEOL, SM6490). Elemental atomic ratio was observed by energy dispersive X-ray technique (EDX). Electrical measurements were done at room temperature using four-probe method (ISO (9001-2000) SVS/NC). Moreover, specific surface area was elucidated by applying BET procedure.

Various electrochemical measurements i.e., cyclic voltammetry (CV), galvanostatic charge-discharge (GCD) and electrochemical impedance spectroscopy (EIS) have been performed by employing Autolab PGSTAT12 workstation and Nova software. A 2M KOH electrolytic

23

solution was employed in the measurement performed using three electrode system (with the platinum-wire as counter electrode, Ag/AgCl as reference electrode, synthesized product on NF as working electrode material). In addition, symmetric behavior of GO supported ZnS nanoweb electrode has also been observed for supercapacitor applications. For the symmetric measurements, both working electrodes were shielded by using filter paper as a separator, and electrodes were sandwiched by gold-plated Cu sheets, which were employed as the current sensor.

5. Acknowledgement

6. References

1. Y. Huang, M. Zhong, F. Shi, X. Liu, Z. Tang, Y. Wang, Y. Huang, H. Hou, X. Xie and C. Zhi, *Angewandte Chemie, Intern.in Eng.* 2017, **56**, 9141-9145.

2. L.-F. Chen, Y. Lu, L. Yu and X. W. Lou, *Energy & Environmental Science*, 2017, **10**, 1777-1783.

3. Y. Qiu, X. Zhang and S. Yang, *Physical Chemistry Chemical Physics*, 2011, **13**, 12554-12558.

4. Y. Liu, G. Jiang, S. Sun, B. Xu, J. Zhou, Y. Zhang and J. Yao, *Journal of Alloys and Compounds*, 2018, **731**, 560-568.

5. L. Hu, M. Pasta, F. L. Mantia, L. Cui, S. Jeong, H. D. Deshazer, J. W. Choi, S. M. Han and Y. Cui, *Nano Lett*, 2010, **10**, 708-714.

6. C. Larson, B. Peele, S. Li, S. Robinson, M. Totaro, L. Beccai, B. Mazzolai and R. Shepherd, *Science*, 2016, **351**, 1071-1074.

7. H. Hu, Bu Y. Guan and Xiong W. Lou, *Chem*, 2016, **1**, 102-113.

24

8.   D. Sheberla, J. C. Bachman, J. S. Elias, C.-J. Sun, Y. Shao-Horn and M. Dinca, *Nat Mater*, 2017, **16**, 220-224.

9.   M. Jana, P. Khanra, N. C. Murmu, P. Samanta, J. H. Lee and T. Kuila, *Physical Chemistry Chemical Physics*, 2014, **16**, 7618-7626.

10.   Y. Liu, G. Jiang, S. Sun, B. Xu, J. Zhou, Y. Zhang and J. Yao, *Journal of Electroanalytical Chemistry*, 2017, **804**, 212-219.

11.   G. Yilmaz, C. X. Guo and X. Lu, *ChemElectroChem*, 2016, **3**, 158-164.

12.   C. Nicolò, R. V. Ricardo, D. Willem, S. Linda, B. Koen, D. V. D. E. and F. Jan, *ChemElectroChem*, 2014, **1**, 1182-1188.

13.   X. Xia, C. Zhu, J. Luo, Z. Zeng, C. Guan, C. F. Ng, H. Zhang and H. J. Fan *Small*, 2014, **10**, 766-773.

14.   H. Chen, G. Jiang, W. Yu, D. Liu, Y. Liu, L. Li, Q. Huang and Z. Tong, *Journal of Materials Chemistry A*, 2016, **4**, 5958-5964.

15.   P. Zhang, B. Y. Guan, L. Yu and X. W. D. Lou, *Angewandte Chemie, Intern.in Eng.*, 2017, **56**, 7141-7145.

16.   M. Khairy and S. A. El-Safty, *Chemical Communications*, 2014, **50**, 1356-1358.

17.   J. Kang, A. Hirata, L. Kang, X. Zhang, Y. Hou, L. Chen, C. Li, T. Fujita, K. Akagi and M. Chen, *Angewandte Chemie*, 2013, **125**, 1708-1711.

18.   M. S. Javed, S. Dai, M. Wang, Y. Xi, Q. Lang, D. Guo and C. Hu, *Nanoscale*, 2015, **7**, 13610-13618.

19.   R. R. Salunkhe, Y. V. Kaneti, J. Kim, J. H. Kim and Y. Yamauchi, *Accounts of Chemical Research*, 2016, **49**, 2796-2806.

20.   Z. Tianye, T. M. H., L. Bei, R. Sijia, L. Ying, G. T. S., L. Kwok-Ho, C. In-Suk and B. S. T., *ChemElectroChem*, 2018, doi:10.1002/celc.201800467.

25

21. H. Huang, J. Zhang, L. Jiang and Z. Zang, *Journal of Alloys and Compounds*, 2017, **718**, 112-115.

22. Z. Zang, X. Zeng, M. Wang, W. Hu, C. Liu and X. Tang, *Sensors and Actuators B: Chemical*, 2017, **252**, 1179-1186.

23. S. S. T. and S. R. Kalai, *ChemElectroChem*, 2015, **2**, 1063-1063.

24. S. Sun, G. Jiang, Y. Liu, Y. Zhang, J. Zhou and B. Xu, *Materials Letters*, 2017, **197**, 35-37.

25. H. Liang, H. Xiang, L. Zhoubin and W. Zhenhai, *ChemElectroChem,* 2018*, doi:10.1002/celc.201800412.

26. R. Rajesh and R. Kwang-Sun, *ChemElectroChem*, 2018, doi:10.1002/celc.201800533.

27. M. F. Iqbal, M. N. Ashiq, A. Razaq, M. Saleem, B. Parveen and M.-U. Hassan, *Electrochimica Acta*, 2018, **273**, 136-144.

28. M. F. Iqbal, H. Mahmood Ul, M. N. Ashiq, S. Iqbal, N. Bibi and B. Parveen, *Electrochimica Acta*, 2017, **246**, 1097-1103.

29. Y. Li and Y. Wu, *Journal of the American Chemical Society*, 2009, **131**, 5851-5857.

30. R. Ramachandran, M. Saranya, P. Kollu, B. P. C. Raghupathy, S. K. Jeong and A. N. Grace, *Electrochimica Acta*, 2015, **178**, 647-657.

31. Y. Wang, A. G. El-Deen, P. Li, B. H. L. Oh, Z. Guo, M. M. Khin, Y. S. Vikhe, J. Wang, R. G. Hu, R. M. Boom, K. A. Kline, D. L. Becker, H. Duan and M. B. Chan-Park, *ACS Nano*, 2015, **9**, 10142-10157.

32. M. S. Javed, J. Chen, L. Chen, Y. Xi, C. Zhang, B. Wan and C. Hu, *Journal of Materials Chemistry A*, 2016, **4**, 667-674.

33. J. Xing, M. Liao, C. Zhang, M. Yin, D. Li and Y. Song, *Physical Chemistry Chemical Physics*, 2017, **19**, 14030-14041.

26

34.   K. Krishnamoorthy, G. K. Veerasubramani, S. Radhakrishnan and S. J. Kim, *Chemical Engineering Journal*, 2014, **251**, 116-122.

35.   P. Simon, Y. Gogotsi and B. Dunn, *Science*, 2014, **343**, 1210-1211.

36.   H. Tong, W. Bai, S. Yue, Z. Gao, L. Lu, L. Shen, S. Dong, J. Zhu, J. He and X. Zhang, *Journal of Materials Chemistry A*, 2016, **4**, 11256-11263.

37.   N. S. Arul, L. S. Cavalcante and J. In Han, *Journal of Solid State Electrochemistry*, 2018, **22**, 303-313.

38.   Y. Zhang, J. Xu, Y. Zheng, Y. Zhang, X. Hu and T. Xu, *Nanoscale Research Letters*, 2017, **12**, 412.

39.   W. Fu, W. Han, H. Zha, J. Mei, Y. Li, Z. Zhang and E. Xie, *Physical Chemistry Chemical Physics*, 2016, **18**, 24471-24476.

40.   M. F. Iqbal, H. Mahmood Ul, M. N. Ashiq, S. Iqbal, N. Bibi and B. Parveen, *Electrochimica Acta*, 2017, **246**, 1097-1103.

41.   L. Lim, Y. Liu, W. Liu, R. Tjandra, L. Rasenthiram, Z. Chen and A. Yu, *ACS Applied Materials & Interfaces*, 2017, **9**, 39576-39583.

42.   R. R. Salunkhe, J. Tang, N. Kobayashi, J. Kim, Y. Ide, S. Tominaka, J. H. Kim and Y. Yamauchi, *Chemical Science*, 2016, **7**, 5704-5713.

43.   P. Wen, M. Fan, D. Yang, Y. Wang, H. Cheng and J. Wang, *Journal of Power Sources*, 2016, **320**, 28-36.

44.   R. B. Pujari, A. C. Lokhande, A. A. Yadav, J. H. Kim and C. D. Lokhande, *Materials & Design*, 2016, **108**, 510-517.

45.   R. Li, S. Wang, Z. Huang, F. Lu and T. He, *Journal of Power Sources*, 2016, **312**, 156-164.

46   X. Meng, J. Deng, J. Zhu, H. Bi, E. Kan and X. Wang, *Scientific Reports*, 2016, **6**, 21717-26.

27

47. X. Li, Q. Li, Y. Wu, M. Rui and H. Zeng, *ACS Applied Materials & Interfaces*, 2015, **7**, 19316-19323.

48. S. Li, C. Yu, J. Yang, C. Zhao, M. Zhang, H. Huang, Z. Liu, W. Guo and J. Qiu, *Energy & Environmental Science*, 2017, **10**, 1958-1965.

49. S. Dai, B. Zhao, C. Qu, D. Chen, D. Dang, B. Song, B. M. deGlee, J. Fu, C. Hu, C.-P. Wong and M. Liu, *Nano Energy*, 2017, **33**, 522-531.

50. X.-Y. Yu, L. Yu, H. B. Wu and X. W. Lou, *Angewandte Chemie International Edition*, 2015, **54**, 5331-5335.

51. A. A. AbdelHamid, X. Yang, J. Yang, X. Chen and J. Y. Ying, *Nano Energy*, 2016, **26**, 425-437.

52. S. J. Patil, J. H. Kim and D. W. Lee, *Journal of Power Sources*, 2017, **342**, 652-665.

53. M. M. Shaijumon, F. S. Ou, L. Ci and P. M. Ajayan, *Chemical Communications*, 2008, 2373-2375.

54. M. S. Javed, S. Dai, M. Wang, D. Guo, L. Chen, X. Wang, C. Hu and Y. Xi, *Journal of Power Sources*, 2015, **285**, 63-69.

Accepted Manuscript